Nano Res. 2011, 4(11): 1099–1109
DOI 10.1007/s12274-011-0164-3
Review Article

ISSN 1998-0124
CN 11-5974/O4

From Proton Conductive Nanowires to Nanofuel Cells: A Powerful Candidate for Generating Electricity for Self-Powered Nanosystems

Caofeng Pan, Jun Luo, and Jing Zhu (✉)

Beijing National Center for Electron Microscopy, Laboratory of Advanced Materials, State Key Laboratory of New Ceramics and Fine Processing, Department of Material Science and Engineering, Tsinghua University, Beijing 100084, China

Received: 15 June 2011 / Revised: 12 July 2011 / Accepted: 13 July 2011
© Tsinghua University Press and Springer-Verlag Berlin Heidelberg 2011

ABSTRACT

The likely goal of nanotechnology is the integration of individual nanodevices into a nanosystem, which includes the nanodevice(s), power harvesting unit, data processing logic system, and possibly wireless communication unit. A nanosystem requires a nanoscale power source to make the entire package extremely small and high performance. The nanofuel and nanobiofuel cells developed here represent a new self-powering approach in nanotechnology, and their power output is high enough to drive nanodevices for performing self-powered sensing. This study shows the feasibility of building self-powered nanosystems for biological sciences, environmental monitoring, defense technology and even personal electronics.

KEYWORDS

Nafion nanowire, nanofuel cell, nanobiofuel cell, self-powered nanosystem

1. Introduction

The goal of nanotechnology is to build nanodevices that are intelligent, multifunctional, exceptionally small, extremely sensitive and with low power consumption. Numerous investigations have resulted in novel nanodevices and applications based on nanomaterials; examples include biosensors [1], resonators [2], transistors [3], logic devices [4], *in situ* real-time biomedical monitoring and detection [5], and optoelectronics [6]. Unfortunately, such devices currently cannot work without an external power supply, and a nanoscale power source is required. Although a battery or energy storage unit is an option for powering nanodevices, harvesting energy from the environment is an essential requirement for building a "self-powered" nanodevice/nanosystem [7], which is an integration of nanodevice(s) and nano-enabled energy scavenging technologies.

There have been several reports of power sources at the nanoscale. A nanogenerator (NG) which converts mechanical energy of both low frequency (~Hz) and high frequency (~50 kHz) into electricity by means of piezoelectric zinc oxide nanowires has been demonstrated [8–14]. A single silicon nanowire-based heterostructure has been used to fabricate a solar cell that is effective for driving a nanowire-based pH sensor or logic gate [15]. Fuel cells have many advantages over conventional batteries, such as rapid recharging and higher stored energy density. The most abundant

Address correspondence to jzhu@mail.tsinghua.edu.cn

energy available in nature or *in vivo* biosystems is chemical and biochemical energy, from fuels such as methanol and glucose. We have reported nanofuel and nanobiofuel cells based on individual proton conductive polymer nanowires (NWs) for converting chemical/biochemical energy, from fuels such as methanol and glucose, into electricity. In the latest work on NW-based nanobiofuel cells, a whole cell was fabricated at the nano/micron scale, and generated an output power as high as 0.5–3 μW in glucose solution, in human blood and in the juice of a watermelon. It was also integrated with a set of NW-based sensors for performing self-powered sensing.

In this review, Section 2 is focused on the synthesis, characterization and excellent proton conductivity of NWs formed from the proton conductive polymer, Nafion® (NFNWs); Section 3 covers nanofuel cells based on the NFNWs with PtRu/C and Pt/C as catalysts, which convert inorganic chemical energy into electricity; Section 4 describes nanobiofuel cells based on the NFNWs with enzymes as catalysts, which convert biochemical energy into electricity; Section 5 focuses on self-powered micro/nano systems, in which several nanodevices have been successfully driven by our NW-based (bio)fuel cells; Section 6 is the conclusion and some perspectives.

2. The synthesis, characterization, and excellent proton conductivity of NFNWs

2.1 NFNWs fabricated by template extrusion method

Nafion® is one of the most common commercial organic materials, and a registered trade mark by DuPont de Nemours (USA) for poly (perfluorosulfonicacid) membranes. The greatest interest in Nafion in recent years derives from its use as a proton conducting membrane in proton exchange membrane fuel cells (PEMFCs), since hydrogen energy is considered as one of the most important new energy resources in the future. Such a proton exchange membrane is the key component in fuel cells, but is also a major obstacle to shrinking the size of a fuel cell. If we could obtain a nanoscale proton conductor, we could build a fuel cell at the nanoscale. Therefore, research on NFNWs should lead to great potential applications for nanofuel cells.

An extrusion method, using anodic aluminum oxide (AAO) membranes (Fig. 1(a)) as templates, has been developed to fabricate NFNW arrays with tunable length and diameter [16–18]. As shown in Fig. 1(b), most of the AAO pores are filled with NWs whose diameters are about 85 nm. Figure 1(c) shows that the NWs (grey contrast) have fully filled the AAO pores (dark contrast) in the radial direction. Due to the confinement of the AAO template, the NFNWs are well aligned. The diameter and the length of the NFNWs can be controlled by changing the pore diameter and the thickness of the AAO templates. Transmission electron microscope (TEM) images of an as-synthesized NFNW with a diameter of about 40 nm are shown in Figs. 1(d) and 1(e). From the TEM images, we can see that the NFNWs obtained via this method are porous. Systematic investigation showed that the NFNWs are formed by absorbing the Nafion molecules onto the AAO pore wall surface. Surface decoration of the templates plays an important role in the synthesis of the

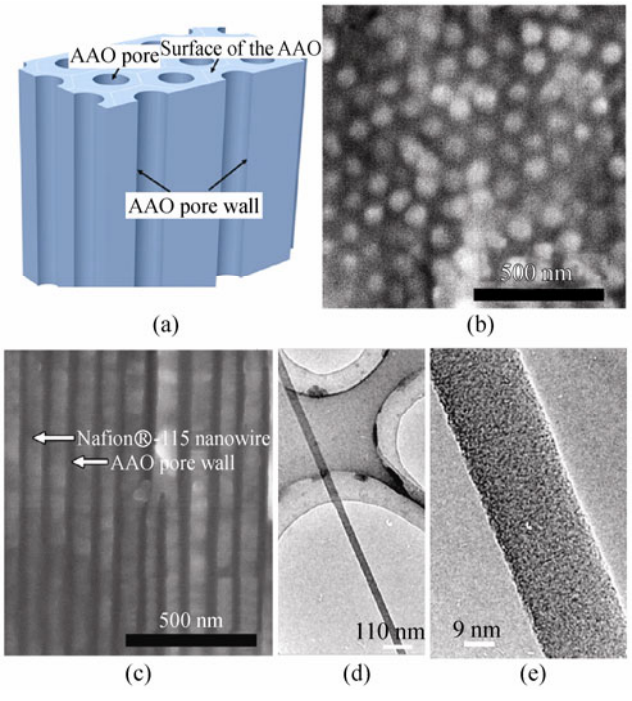

Figure 1 (a) Three-dimensional (3D) model of an AAO template. (b and c) Scanning electron microscope (SEM) images, where (b) is the top view and (c) is the cross-sectional view of an as-synthesized Nafion®-115 NW arrays in the AAO pores. (d and e) TEM images of an as-synthesized NFNW: (d) Low magnification and (e) high magnification. Reprinted with permission from [17]. Copyright 2007, IOP Publishing Ltd

NFNW arrays. By using sodium dodecyl sulfate (SDS) as a surfactant in the surface decoration, the filling rate of the NFNWs in the template exceeds 95%, compared with a filling rate of only 42% in an undecorated template [17].

2.2 NFNWs fabricated by electrospinning

Although the aforementioned template-directed method provides a straightforward and reliable strategy for processing Nafion into nanostructures with one-dimensional (1D) morphologies, it involves multiple (at least three) steps: the fabrication of templates, the filling of the templates with Nafion, and finally the selective removal of the templates. It will clearly be an advantage if one can develop a simpler method that is capable of generating Nafion nanofibers in one step and in larger quantities. Electrospinning represents a relatively simple and versatile method for generating polymer nanostructures [19–21]. In the continuous-feeding mode, numerous copies of NWs can be formed within a few seconds. In a typical process, shown in Fig. 2(a), a Nafion/poly(vinyl pyrrolidone) (PVP) solution was injected from a small syringe tip under the influence of an electric field as strong as several kV/cm. The needle was connected to a high voltage of 16 kV, while the distance between the needle tip and the collector was fixed at 10 cm during electrospinning. The collector was a piece of flat aluminum foil. The as-spun NWs were left in air for 5 h to allow the solvent to be vaporized completely. Figure 2(b) shows a SEM image of NFNWs electrospun from an ethanol solution containing PVP and Nafion. (We also denote Nafion/PVP NWs as NFNWs, since the percentage of PVP is very low and PVP does not affect the proton conductivity of the wire.) Each individual nanowire is uniform in cross section. The diameter of the NFNWs varies from 200 nm to several microns and the length can reach several centimeters. The diameters of the Nafion nanowires could be controlled by varying a series of electrospinning parameters, such as feeding rate and applied voltage (Figs. 2(e)–2(f)). The diameter of the NFNW increases with increasing feeding rate (Fig. 2(e)). At low feeding rates (for example, 15 standard cubic centimeters per minute (sccm)), the diameter is influenced by the electrospinning voltage, but at high feeding rates (like 30 sccm), there is an optimum voltage to obtain smaller diameter NFNWs, which is about 20 kV in our experiment.

Double parallel conductive electrodes can be used instead of aluminum film in order to obtain well-oriented NFNW arrays. The distance between the two conductive electrodes can be varied from hundreds of microns to several centimeters. Figure 2(c) shows an optical micrograph of NFNWs that were collected with two conductive electrodes. Figure 2(d) shows the distribution of the angle (θ) between the long axes of the NFNWs in Fig. 2(c) and their expected direction. It

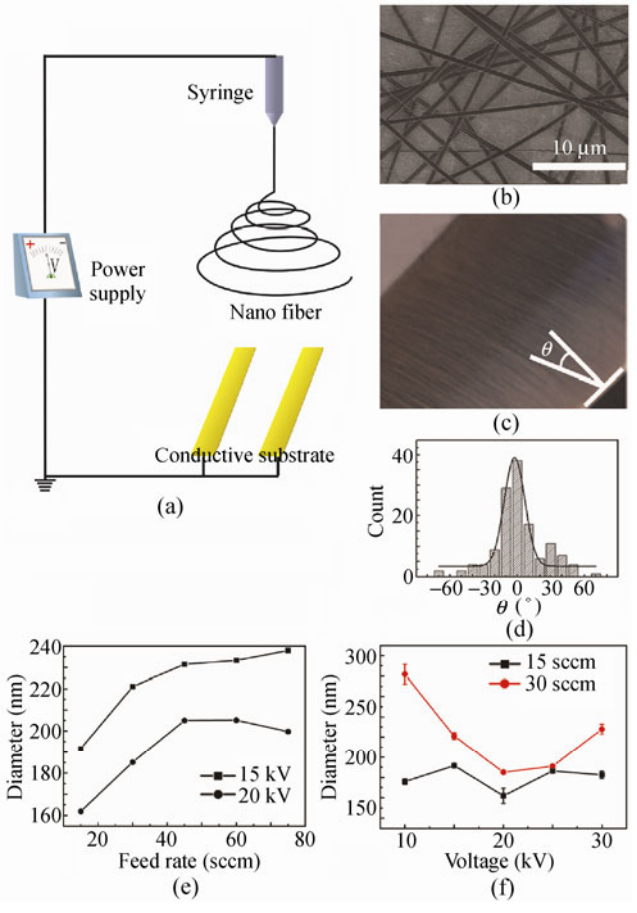

Figure 2 (a) Schematic illustration of the electrospinning setup that we used to generate uniaxially aligned NWs. The collector here contained two pieces of conductive aluminum strips. (b) SEM image of NFNWs collected by aluminum foil. (c) Optical micrograph of NFNWs collected by two parallel aluminum electrodes. (d) Distribution of the angle (θ) between the long axes of the NFNWs and their expected direction. θ is defined in (c). (e)–(f) Effect of varying the electrospinning parameters (feeding rate and electrospinning voltage) on the diameter of nanowires. Reprinted with permission from [22]. Copyright 2010, Wiley–VCH

indicates clearly that the NFNWs are uniaxially aligned across the gap with their longitudinal axes perpendicular to the edges of the gap. In contrast, the NFNWs collected by an Al film (Fig. 2(b)) are essentially disordered in spatial orientation.

Chen et al. [22] and Dong et al. [23] also reported the fabrication of high purity Nafion nanofibers via electrospinning. Unlike previous work, which required a high amount (> 12 wt.%) of carrier polymer to induce polymer chain entanglement for the electrospinning of Nafion fibers, they obtained Nafion fibers with the use of only 0.1 wt.% carrier polymer (i.e., 99.9 wt.% Nafion). Figures 3(a)–3(e) show the effect of increasing the Nafion content in the nanofibers from 98 to 99.9 wt.%. Only beaded fibers was obtained if lower molecular mass PEO (M_w 400 kg/mol) and 99.9 wt.% Nafion was used as precursor solutions (Fig. 3(f)). Figure 3(g) shows the effect of fiber composition on fiber diameter, where the average fiber diameter increased from 125 nm (98 wt.% Nafion) to 400 nm (99.9 wt.% Nafion).

2.3 Characterization of NFNWs

To evaluate whether the as-prepared NFNWs still have good proton transportation properties or not, a comprehensive structure characterization, including energy dispersive X-ray (EDX), and infrared (IR) and Raman spectroscopy, was carried out.

The SEM morphology shows that a NFNW has a homogeneous diameter, and the EDX spectrum indicates that the NFNWs consist of C, O, F, and S elements only [24].

IR and Raman spectra of a Nafion membrane and as-prepared NFNWs are shown in Figs. 4(a) and 4(b), respectively. The positions of the Nafion peaks in the Raman and IR spectra of the NFNWs and the Nafion precursor are consistent with each other over the whole range of wavenumber employed [18, 25]. This demonstrates that the Nafion structure in the as-synthesized NFNWs does not change after the electrospinning process.

2.4 Size-dependent proton conductivity of NFNWs

Proton conductivity is very important for NFNWs since they are expected to be used for nanofuel cells. Hence, the proton conductivity of individual NFNWs was measured. A size dependence of the proton

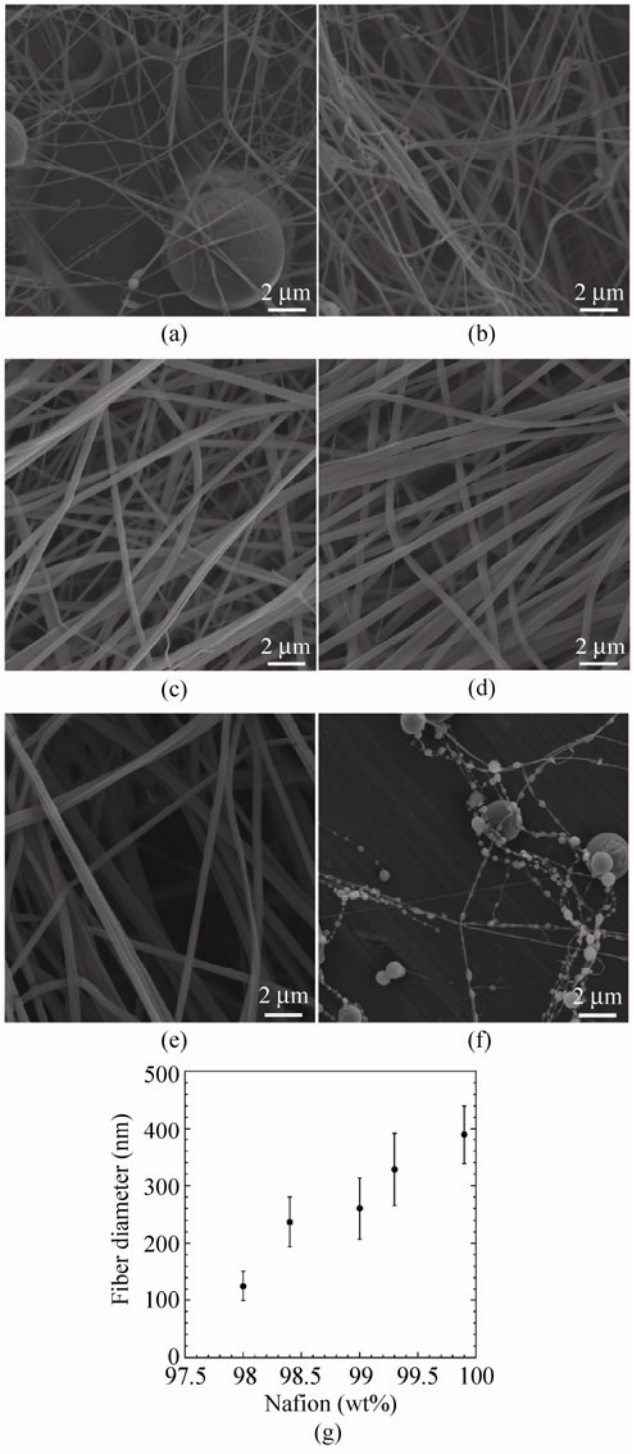

Figure 3 SEM images of high purity Nafion nanofibers electrospun with high molecular mass poly(ethylene oxide) (PEO) (M_w 8000 kg/mol) at fiber compositions of (a) 98, (b) 98.4, (c) 99, (d) 99.3, (e) 99.9 wt.% Nafion. (f) Beaded fibers produced with solutions with lower molecular mass PEO (M_w 400 kg/mol) and 99.9 wt.% Nafion. (g) Fiber diameter as a function of fiber composition in wt.% Nafion. Reprinted with permission from [23]. Copyright 2010, American Chemical Society

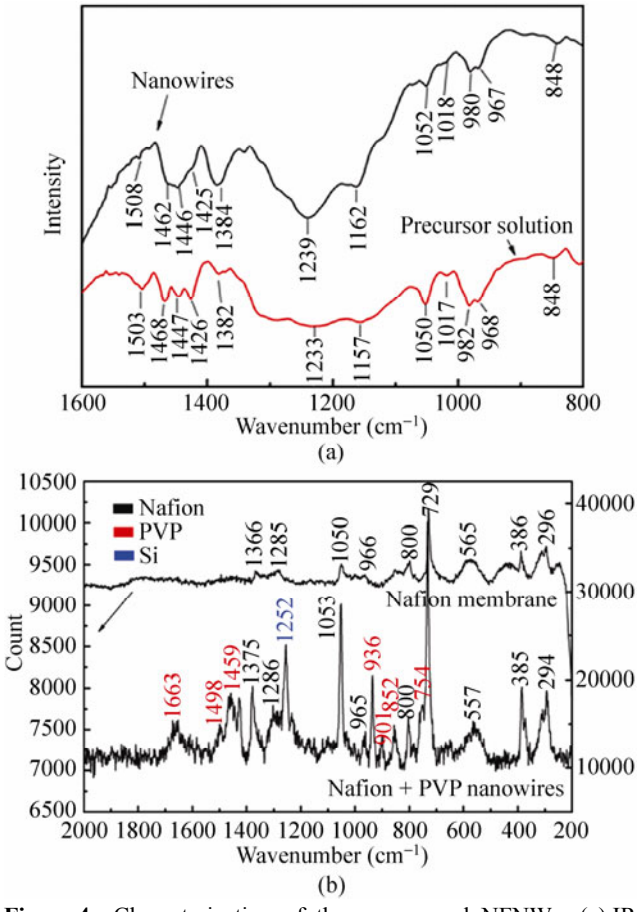

Figure 4 Characterization of the as-prepared NFNWs. (a) IR spectra of the NFNWs and a Nafion precursor solution. (b) Raman spectra of the NFNWs and a Nafion membrane. Reprinted with permission from [25]. Copyright 2008, Wiley–VCH

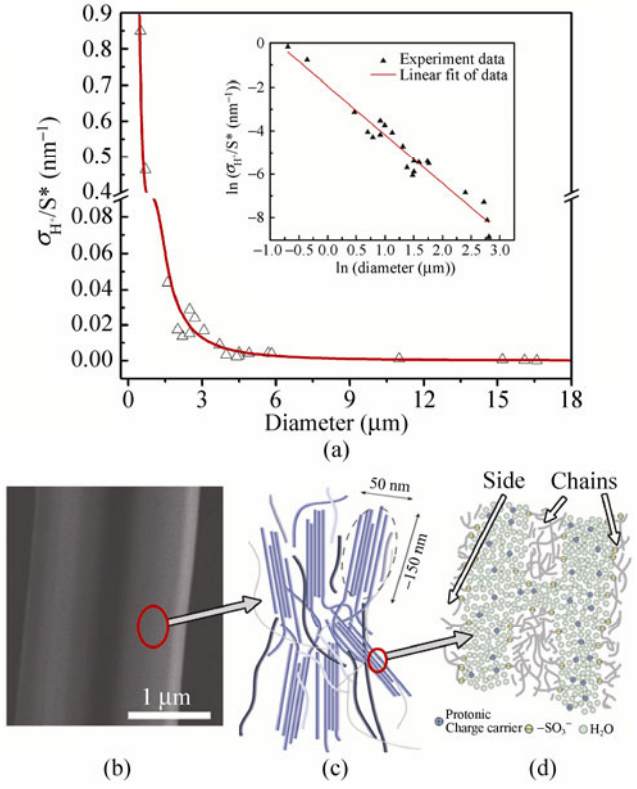

Figure 5 Size dependence of the proton conductivity. (a) Diameter dependence of the proton conductivity (σ_{H^+}) of individual NFNWs when the diameter ranges from 500 nm to 16.6 μm. The inset shows the good linear relationship between log (σ_{H^+}) and log (d), where d denotes the diameter of NFNWs. (b) SEM image of a single NFNW with a diameter of about 1.91 μm. (c) Schematic representation of an entangled network of elongated rod-like aggregates in a NFNW, where the aggregates show a tendency to lie parallel along the NFNW axis. (d) Stylized view of the nanoscopic proton transport channel formed by the sulfonic groups in the NFNW, showing that the proton transport channels parallel to the NFNW axis are dominant. Reprinted with permission from [25]. Copyright 2008, Wiley–VCH

conductivity of the NFNWs with diameter ranging from 500 nm to 16.6 μm was observed experimentally, as shown in Fig. 5(a). When the NFNW diameter was smaller than 2.5 μm, the measured proton conductivity increased dramatically with decreasing diameter and was significantly higher than that in a Nafion membrane [26]. It is interesting to note that the double logarithmic plot of the proton conductivity versus the diameter shows a good linear relationship in the diameter range from 500 nm to 16.6 μm.

The size-dependence of the proton conductivity can be attributed to the change in the assembly of Nafion molecules during the fabrication process. Figure 5(b)–5(d) is a multilevel view of the nanoscopic proton transport channel formed by the sulfonic groups in NPNWs. A Nafion molecule is considered to be rod-like in the precursor solution [27], and a preferred microstructural orientation may be introduced during the electrospinning process, as shown in Fig. 5(c). The rod-like Nafion molecules in a NFNW try to lie parallel to the NFNW axis direction, giving a "texture", due to the confinement of the NFNW diameter. Further, the degree of texture increases when the NFNW diameter decreases [28].

Dong et al. confirmed this result by comparing the 2D X-ray scattering patterns of both macroscopically aligned Nafion NWs and cast Nafion films [23]. Figures 6(a) and 6(b) show 2D X-ray patterns of aligned Nafion nanofibers and a Nafion cast film, respectively. The Nafion fibers and the cast film have scattering maxima at q ~1.65 and 1.58 nm^{-1}, respectively, indicating the presence of ionic aggregates. Figure 6(c) shows

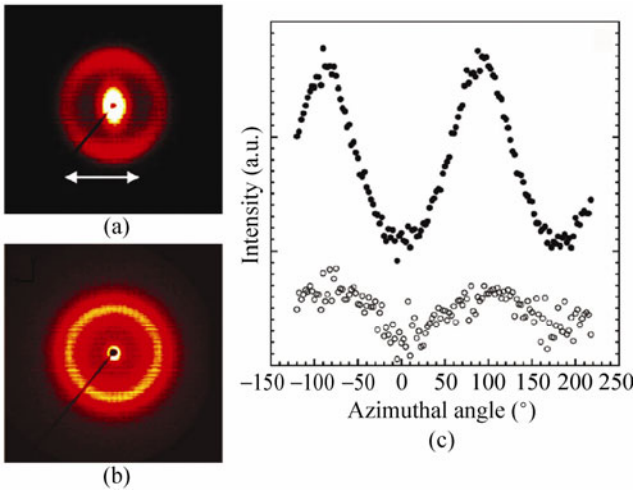

Figure 6 2D X-ray scattering patterns (at 86% relative humidity, 25 ˚C) of (a) macroscopically aligned high purity Nafion nanofibers (the arrows indicate the longitudinal direction of the fibers) and (b) Nafion cast film; (c) X-ray scattering intensity as a function of azimuthal angle for macroscopically aligned high purity Nafion nanofibers (solid symbols) and a cast Nafion film (open symbols). Reprinted with permission from [23]. Copyright 2010, American Chemical Society

the scattering intensity as a function of azimuthal angle and clearly indicates that the ionic aggregates are isotropic in the cast film (as expected) and anisotropic in the nanofibers. The scattering data from the electronspun nanofibers are consistent with the presence of anisotropic ionic aggregates oriented along the nanofiber axis direction. They also found that the nanofibers exhibited strong anisotropic scattering at smaller angles (which appears white in Fig. 6(a)), which can be attributed to form factor scattering from the interstitial spaces between nanofibers in the porous mat.

As a result, within such an optimized structure of NFNWs, proton transport from anode to cathode is easier and faster. This is the reason why the NFNW proton conductivity increases dramatically with decreasing NFNW diameter.

3. NFNW-based nanofuel cells

A nanofuel cell can be fabricated at the nano/submicron scale taking advantage of the excellent proton conductivity of the NFNWs. The performance of the as-built nanofuel cell is enhanced by orders of magnitude compared with traditional fuel cells [24]. Figure 7(a) illustrates the design of our nanofuel cells: a NFNW lies on a substrate, and two electrodes are deposited at either end of the NFNW. Then a SiO_2 strip is deposited in the middle, in order to separate the anode and the cathode zones. PtRu/C and Pt/C are dispersed subsequently onto the NFNWs to act as catalysts in the anode and the cathode zones, respectively. When the cell is filled with a fuel (such as methanol), a chemical reaction occurs: the methanol is oxidized and releases protons and electrons, and the protons are transported to the cathode via the NFNW, while the electrons are transported around the external circuit, providing the devices with energy (Fig. 7(b)).

The typical output performance of an experimental nanofuel cell is shown in Figs. 7(c) and 7(d). The short circuit current is about 3.5 μA (Fig. 7(c)), and the output of the nanofuel cell is very stable, as indicated by the four series of measurements. The open circuit voltage is about 178 mV, directly measured by a multimeter (Fig. 7(d)). A comprehensive study of the voltage–current and power–current performances is shown in Fig. 7(e). The nanofuel cell generates an open circuit voltage (OCV) of 314 mV, a maximum current density (I_d) of about 1.21 μA/μm^2 (at zero applied load), and a maximum power density (P_n) of about 0.095 μW/μm^2 at room temperature (see the black curve in Fig. 7(e)). Compared to the performance at room temperature, that at 333 K (see the red curve in Fig. 7(e)) is enhanced dramatically with an increased OCV of over 100 mV, the maximum I_d (at zero applied load) increased three-fold and maximum P_n of 0.348 μW/μm^2.

4. NFNW-based nanobiofuel cells

The most abundant energy available in biosystems is chemical and biochemical energy, such as glucose. Harvesting chemical energy in biofluids can be a powerful approach to fabricate sustainable, independent, mobile and self-powered nanodevices for *in vivo* biosensing. A nanobiofuel cell (NBFC) based on a single NFNW for converting chemical energy from a biofluid such as glucose/blood into electricity has been reported by us [29]. The glucose is supplied by A biofluid, and the NFNW serves as the proton conductor.

Our NBFC is based on an electrochemical process converting glucose into gluconolactone. As shown in

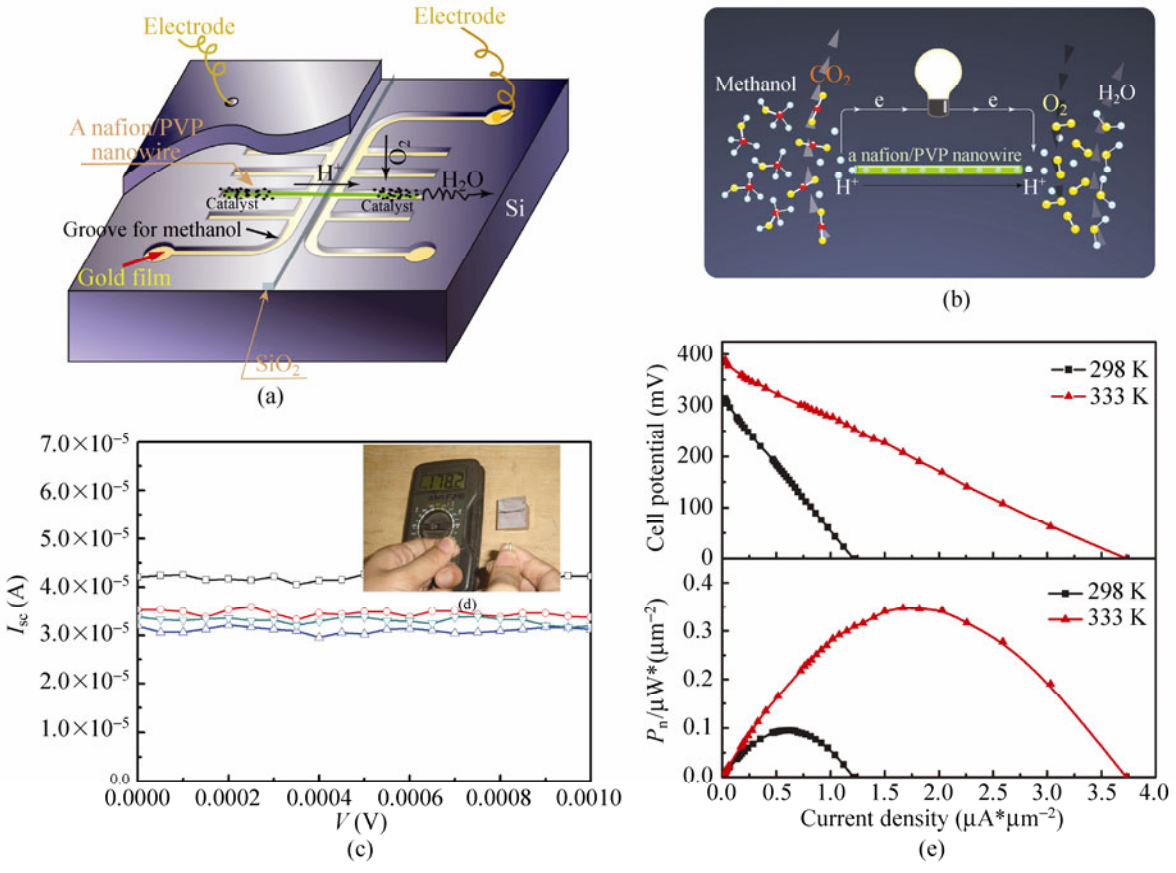

Figure 7 Design and performance of the nanofuel cell. (a) Schematic illustration of the structure of a nanofuel cell. The groove (with a 50 nm Au film on it) on the Si substrate serves simultaneously as fuel container and electrode. (b) Working principles of the nanofuel cell. (c) The short circuit current (I_{sc}) of an experimental nanofuel cell, and the very stable output of the tested nanofuel cell as indicated by four series of measurements. (d) Photograph of the cell used to obtain the data in (c), showing an open circuit voltage of about 178 mV. (e) Performance at 298 K and 333 K of a nanofuel cell based on a NFNW with a diameter of ~2.1 μm, indicating that the performance improves with increasing temperature. Fuel: 0.1 mol/L methanol/1.0 mmol/L H_2SO_4; Oxidant: air. The data in (c) and (d) are obtained from the same nanofuel cell, and the data in (e) are obtained from a different nanofuel cell. Reprinted with permission from [25]. Copyright 2008, Wiley–VCH

Fig. 8(a), glucose oxidase (GO_x) and laccase are used as catalysts at the anode and cathode, respectively. GO_x is an enzyme that catalyzes the oxidation of *β-D*-glucose by molecular oxygen, while laccase is an enzyme that catalyses the reduction of oxygen into water. When the NBFC is in contact with a biofluid that contains glucose, the chemical processes occurring at the two ends of the NW are as shown in Fig. 8(b): glucose is electrooxidized to gluconolactone at the anode (Eq. 1) [30] and dissolved O_2 is electroreduced to water at the cathode (Eq. 2) [31, 32].

Anode:

$$\text{Glucose} \xrightarrow{GO_x} \text{Gluconolactone} + 2H^+ + 2e^- \quad (1)$$

Cathode:

$$\frac{1}{2}O_2 + 2H^+ + 2e^- \xrightarrow{\text{Laccase}} H_2O \quad (2)$$

The performance of the NBFCs can be characterized by measuring the short circuit current I_{sc} and the open circuit voltage V_{oc}. The output of the NBFCs is in the range of microamperes and tens of millivolts, as shown in Figs. 8(c) and 8(d). The criteria of switching polarity and linear superposition [10, 33] were carried out to verify the received signals. A positive voltage/current is recorded when the current meter is forward connected. For this NBFC, the short-circuit current is 6.9 μA (Fig. 8(c)). When the current meter is reversely

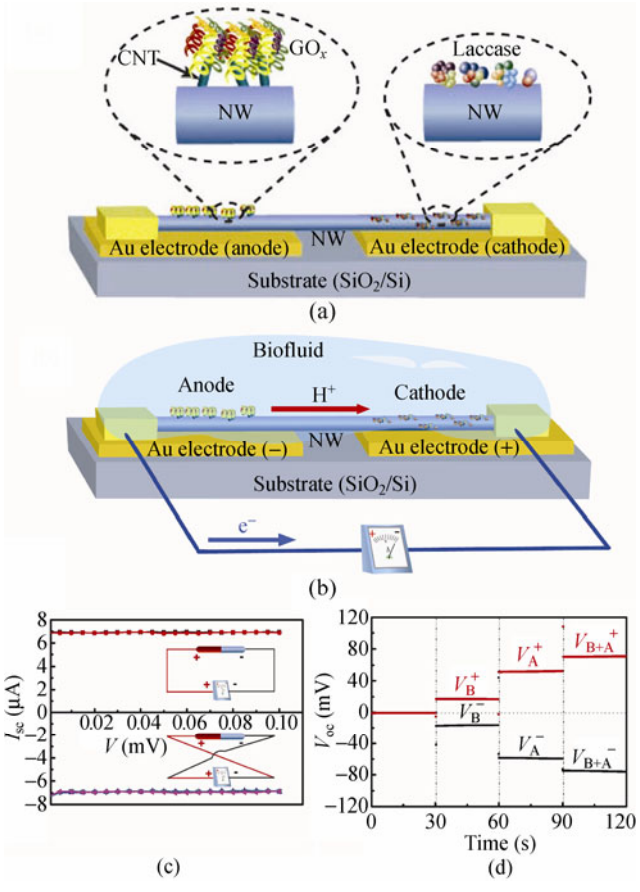

Figure 8 Design and performance of a NBFC based on a single NFNW. (a) Schematic image of the design of the NBFC, where the NFNW lies on a substrate (of any kind) and its two ends are tightly bonded to the substrate and the outlet interconnects. GO_x and laccase are used as catalysts in the anode and the cathode regions, respectively. CNT denotes carbon nanotube. (b) Schematic image of the working principle of the NBFC after it is immersed into a biofuel solution, where chemical reactions occur in the anode and the cathode regions and create a corresponding chemical potential drop along the NFNW. The potential drop drives the flow of protons in the NFNW and electrons through the external load. (c) Test of switching polarity on an experimental NBFC. I_{sc} is about 6.9 μA in the forward-connected configuration (up region) and about –6.9 μA in the reverse-connected (down region). The measurement of I_{sc} is repeated several times, showing a good stability of the NBFC. (d) Superposition of the open-circuit voltage of two NBFCs by connecting them in series. The measurement demonstrates the ability of the NBFC to "add up" or "cancel out". Reprinted with permission from [22]. Copyright 2010, Wiley–VCH

connected, the voltage and current signals are reversed in sign but retain the same magnitudes (Fig. 8(c)). A typical linear superposition experiment is shown in Fig. 8(d): When two NBFCs are connected in series with the same polarity, the open circuit voltage is apparently increased, and the output is close to the sum of the open circuit voltage of the individual NBFCs. In summary, the switching polarity and the linear superposition tests confirm that the outputs are indeed generated by the NBFCs.

The electrical output of the NBFC also depends on the working conditions, such as the concentration and the pH of the glucose solution, and the working temperature. When the concentration of glucose solutions was varied from 0.5 to 10 wt.%, the output performance of the NBFC was relatively high. The I_{sc} varied from 14 to 31 μA with a peak value at a glucose concentration of about 0.5–2 wt.%, which is similar to blood glucose concentration (Fig. 9(a)). Working temperature is another key factor. The NBFCs were tested at temperatures of 20 to 80 ℃, and showed an output peak at 50–70 ℃. (Fig. 9(b)). Although the performance of the NBFC at 37 ℃ (i.e., human body temperature) is lower than that at 70 ℃, the I_{sc} is still as high as 29 μA, which is sufficient to power small devices. In addition to fuel concentration and temperature, pH is also a very important factor affecting the NBFC, since the activity of enzymes varies dramatically with pH (Fig. 9(c)). The NBFC gave a good output in the pH range from 5.0 to 7.2. In view of the above results, it can be concluded that the NBFC have good flexibility for *in vivo* applications.

The performance of NBFCs interfacing directly with biofuels in the human body is important for exploring potential application of NBFCs in powering *in vivo* wireless nanodevices. Figures 9(d) and 9(e) show the performances of our NBFCs operated in neutral glucose-containing phosphate buffer (PBS, pH 7.0) and human blood. It can be seen that V_{oc} in the glucose/PBS solution is about 0.23 V, a little lower than the ideal V_{oc} of a biofuel cell (0.7 V) [34]. The power of the NBFC driven by blood glucose is 0.5 μW, which is 35%–40% of that obtained in the glucose/PBS solution. This decrease can be attributed to partial enzyme inhibition by several compounds present in human blood. Many organic compounds and inorganic ions present in human blood, such as white and red blood cells, urea, HCO_3^-, Mg^{2+}, and Ca^{2+}, could affect the specific activity of the enzymes [35].

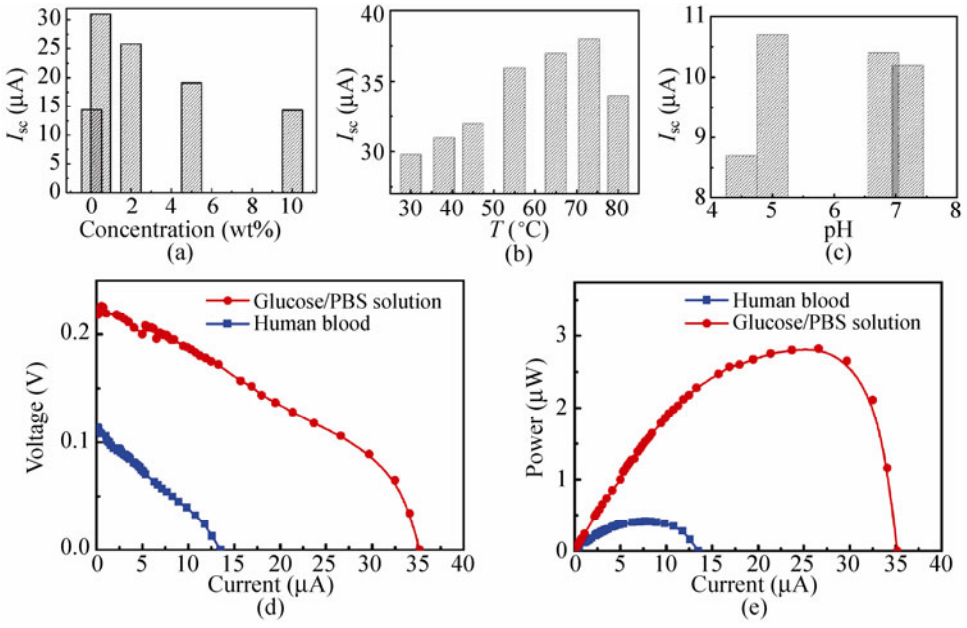

Figure 9 Study of the adaptability and flexibility of NBFC for potential *in vivo* applications. Dependence of the performance of a NBFC on the glucose concentration (a), the working temperature (b), and pH (c) of the biofuel solution. (d), (e) Performance of NBFC in glucose/PBS solution and human blood. The data in (a) and (b) are acquired from the same NBFC; the data in (c) are from a second NBFC, and data in (d) and (e) are from a third NBFC. Reprinted with permission from [22]. Copyright 2010, Wiley–VCH

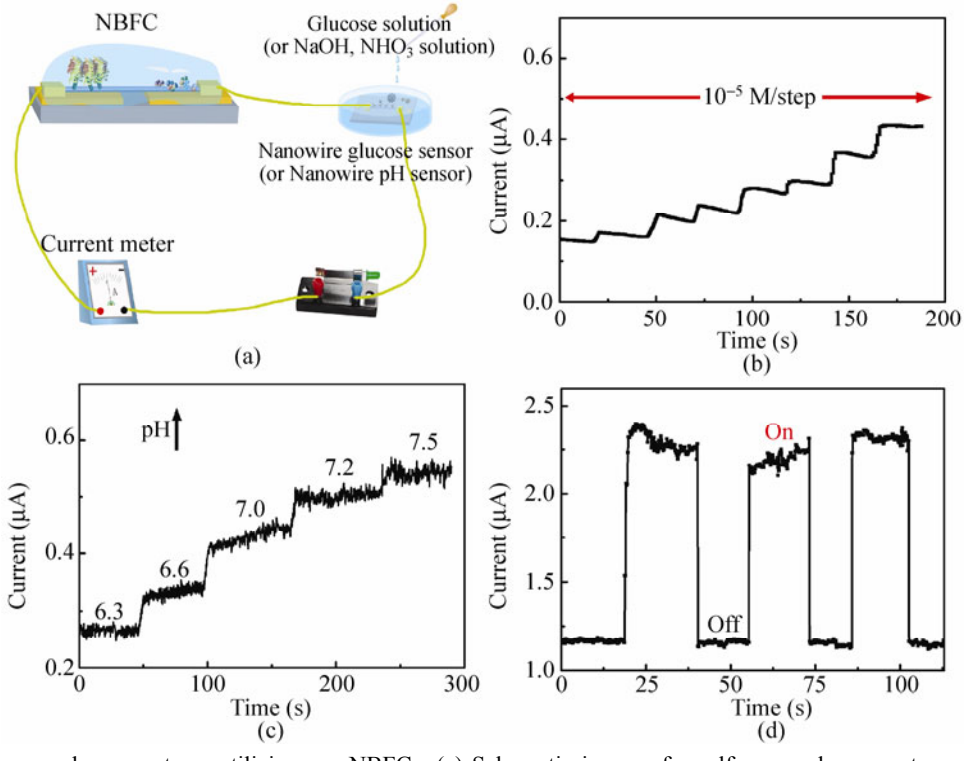

Figure 10 Self-powered nanosystems utilizing our NBFCs. (a) Schematic image of a self-powered nanosystem, where a NBFC, a nanosensor and a current meter are connected in series and the only power source to drive the nanosensor is the NBFC. (b) Current response of a glucose nanosensor driven by a NBFC. An obvious amperometric response as a function of time can be seen when the glucose solution is added into the PBS solution drop by drop. (c) Current response of a pH nanosensor driven by a NBFC. The current increases when the pH increases, and decreases with decreasing pH (not shown here), as indicated by the flat steps. (d) Current response of a CNT-based photon nanosensor, which is sensitive to the switching on and off of visible light, driven by a NBFC. Reprinted with permission from [22]. Copyright 2010, Wiley–VCH

5. Self-powered nanosystems

A NBFC can be integrated with a nanosensor based on a single NW for building a self-powered nanosystem, which typically requires an operation power as low as a few nW. A self-powered nanosystem which can contain a glucose sensor, pH sensor or photon sensor is shown in Fig. 10(a). For the glucose sensor, a rapid and obvious amperometric response is exhibited with successive addition of glucose solution, as shown in Fig. 10(b). The current response of the pH sensor driven by a NBFC is shown in Fig. 10(c). NaOH solution was used to modify the pH of the solution which was monitored in real time by a pH meter. The current increases when the pH is increased step by step because the conductance of the pH sensor varies in different pH solutions. Figure 10(d) shows a CNT-based photon nanosensor driven by a NBFC. An obvious amperometric response is observed when the light is turned on. These results show that the NBFCs successfully serve as a power source for driving not only *in vivo* nanosensors but also other devices.

6. Conclusions

A template extrusion and an electrospinning method have been developed to fabricate NFNW arrays. The diameter of the NFNWs varies between tens of nanometers and several microns, while their length can reach several centimeters. It is found experimentally that the proton conductivity of individual NFNWs is diameter-dependent and much higher than that of the traditional Nafion film, and increases dramatically with decreasing NW diameter when the diameter is smaller than 2.5 μm, following a power law.

By virtue of the excellent proton conductivity of the as-synthesized NFNWs, nanofuel and nanobiofuel cells based on the NFNWs can be realized, and one (bio)fuel cell can be fabricated on an individual NFNW. The best performance of the nanofuel cells corresponds to an open circuit voltage of 430 mV, a maximum current density of about 4.33 $\mu A/\mu m^2$ and a power density of 0.44 $\mu W/\mu m^2$, and such an output is orders of magnitude greater than that of a traditional fuel cell. In the nanobiofuel cells, the electricity can be produced from biofluids, like blood glucose, and the best power output can reach 0.5–3 μW, sufficient to serve as a power source for *in vivo* self-powered nanodevices. By integrating a NBFC with a glucose sensor, a pH sensor or a photon sensor, a self-powered nanosystem has been demonstrated.

This work provides a new approach for self-powered nanotechnology, which harvests electricity from the environment, with applications—such as implantable biomedical devices, wireless sensors, and even portable electronics—that are important in biological science, environmental monitoring, defense technology, and even personal electronics. In the future, it will be crucial to build up self-powered nanosystems with our nanofuel cells, so that they can operate wirelessly, remotely, and independently with a sustainable energy supply.

Acknowledgements

The authors thank the National Program on key Basic Research Project (973 Program), the Chinese National Natural Science Foundation, and the National Centre for Nanoscience and Technology of China for support. This work made use of the resources of the Beijing National Center for Electron Microscopy.

References

[1] Zheng, G. F.; Patolsky, F.; Cui, Y.; Wang, W. U.; Lieber, C. M. Multiplexed electrical detection of cancer markers with nanowire sensor arrays. *Nat. Biotechnol.* **2005**, *23*, 1294–1301.

[2] Bai, X. D.; Gao, P. X.; Wang, Z. L.; Wang, E. G. Dual-mode mechanical resonance of individual ZnO nanobelts. *Appl. Phys. Lett.* **2003**, *82*, 4806–4808.

[3] Zheng, G. F.; Lu, W.; Jin, S.; Lieber, C. M. Synthesis and fabrication of high-performance *n*-type silicon nanowire transistors. *Adv. Mater.* **2004**, *16*, 1890–1893.

[4] Wu, W. Z.; Wei, Y. G.; Wang, Z. L. Strain-gated piezotronic logic nanodevices. *Adv. Mater.* **2010**, *22*, 4711–4715.

[5] Gross, S.; Gilead, A.; Scherz, A.; Neeman, M.; Salomon, Y. Monitoring photodynamic therapy of solid tumors online by BOLD-contrast MRI. *Nat. Med.* **2003**, *9*, 1327–1331.

[6] Duan, X. F.; Huang, Y.; Agarwal, R.; Lieber, C. M. Single-nanowire electrically driven lasers. *Nature* **2003**, *421*, 241–245.

[7] Wang, Z. L. Self-powered nanotech-nanosize machines need still tinier power plants. *Sci. Am.* **2008**, *298*, 82–87.

[8] Qin, Y.; Wang, X. D.; Wang, Z. L. Microfibre-nanowire

hybrid structure for energy scavenging. *Nature* **2008**, *451*, 809–813.

[9] Xu, S.; Qin, Y.; Xu, C.; Wei, Y. G.; Yang, R. S.; Wang, Z. L. Self-powered nanowire devices. *Nat. Nanotechnol.* **2010**, *5*, 366–373.

[10] Yang, R. S.; Qin, Y.; Dai, L. M.; Wang, Z. L. Power generation with laterally packaged piezoelectric fine wires. *Nat. Nanotechnol.* **2009**, *4*, 34–39.

[11] Wang, X. D.; Song, J. H.; Liu, J.; Wang, Z. L. Direct-current nanogenerator driven by ultrasonic waves. *Science* **2007**, *316*, 102–105.

[12] Wang, Z. L.; Song, J. H. Piezoelectric nanogenerators based on zinc oxide nanowire arrays. *Science* **2006**, *312*, 242–246.

[13] Zhu, G. A.; Yang, R. S.; Wang, S. H.; Wang, Z. L. Flexible high-output nanogenerator based on lateral ZnO nanowire array. *Nano Lett.* **2010**, *10*, 3151–3155.

[14] Hu, Y. F.; Zhang, Y.; Xu, C.; Zhu, G. A.; Wang, Z. L. High-output nanogenerator by rational unipolar assembly of conical nanowires and its application for driving a small liquid crystal display. *Nano Lett.* **2010**, *10*, 5025–5031.

[15] Tian, B. Z.; Zheng, X. L.; Kempa, T. J.; Fang, Y.; Yu, N. F.; Yu, G. H.; Huang, J. L.; Lieber, C. M. Coaxial silicon nanowires as solar cells and nanoelectronic power sources. *Nature* **2007**, *449*, 885–889.

[16] Zhang, L.; Pan, C. F.; Zhu, J. Growth mechanism and optimized parameters to synthesize Nafion-115 nanowire arrays with anodic aluminium oxide membranes as templates. *Chinese Phys. Lett.* **2008**, *25*, 3056–3058.

[17] Pan, C. F.; Zhang, L.; Zhu, J.; Luo, J.; Cheng, Z. D.; Wang, C. Surface decoration of anodic aluminium oxide in synthesis of Nafion(R)-115 nanowire arrays. *Nanotechnology* **2007**, *18*, 015302.

[18] Zhang, L.; Pan, C. F.; Zhu, J.; Wang, C. Synthesis and characterization of Nafion(R)-115 nanowire arrays. *Nanotechnology* **2005**, *16*, 2242–2244.

[19] Wu, H.; Lin, D. D.; Zhang, R.; Pan, W. Oriented nanofibers by a newly modified electrospinning method. *J. Am. Ceram. Soc.* **2007**, *90*, 632–634.

[20] Wu, H.; Zhang, R.; Liu, X. X.; Lin, D. D.; Pan, W. Electrospinning of Fe, Co, and Ni nanofibers: synthesis, assembly, and magnetic properties. *Chem. Mater.* **2007**, *19*, 3506–3511.

[21] Li, D.; Xia, Y. N. Electrospinning of nanofibers: reinventing the wheel? *Adv. Mater.* **2004**, *16*, 1151–1170.

[22] Pan, C. F.; Fang, Y.; Wu, H.; Ahmad, M.; Luo, Z. X.; Li, Q.; Xie, J. B.; Yan, X. X.; Wu, L. H.; Wang, Z. L.; Zhu, J. Generating electricity from biofluid with a nanowire-based biofuel cell for self-powered nanodevices. *Adv. Mater.* **2010**, *22*, 5388–5392.

[23] Chen, H.; Snyder, J. D.; Elabd, Y. A. Electrospinning and solution properties of Nafion and poly(acrylic acid). *Macromolecules* **2008**, *41*, 128–135.

[24] Dong, B.; Gwee, L.; Salas-de la Cruz, D.; Winey, K. I.; Elabd, Y. A. Super proton conductive high-purity Nafion nanofibers. *Nano Lett.* **2010**, *10*, 3785–3790.

[25] Pan, C. F.; Wu, H.; Wang, C.; Wang, B.; Zhang, L.; Chen, Z. D.; Hu, P.; Pan, W.; Zhou, Z. Y.; Yang, X.; Zhu, J. Nanowire-based high performance "micro fuel cell": one nanowire, one fuel cell. *Adv. Mater.* **2008**, *20*, 1644–1648.

[26] Gruger, A.; Regis, A.; Schmatko, T.; Colomban, P. Nanostructure of Nafion (R) membranes at different states of hydration-an IR and Raman study. *Vib. Spectrosc.* **2001**, *26*, 215–225.

[27] Alberti, G.; Casciola, M. Solid state protonic conductors, present main applications and future prospects. *Solid State Ionics* **2001**, *145*, 3–16.

[28] Ha, S.; Adams, B.; Masel, R. I. A miniature air breathing direct formic acid fuel cell. *J. Power Sources* **2004**, *128*, 119–124.

[29] Rubatat, L.; Rollet, A. L.; Gebel, G.; Diat, O. Evidence of elongated polymeric aggregates in Nafion. *Macromolecules* **2002**, *35*, 4050–4055.

[30] Delumleywoodyear, T.; Rocca, P.; Lindsay, J.; Dror, Y.; Freeman, A.; Heller, A. A. Polyacrylamide-based redox polymer for connecting redox centers of enzymes to electrodes. *Anal. Chem.* **1995**, *67*, 1332–1338.

[31] Trudeau, F.; Daigle, F.; Leech, D. Reagentless mediated laccase electrode for the detection of enzyme modulators. *Anal. Chem.* **1997**, *69*, 882–886.

[32] Barton, S. C.; Kim, H. H.; Binyamin, G.; Zhang, Y. C.; Heller, A. The "wired" laccase cathode: High current density electroreduction of O-2 to water at +0.7 V (NHE) at pH 5. *J. Am. Chem. Soc.* **2001**, *123*, 5802–5803.

[33] Yang, R. S.; Qin, Y.; Li, C.; Dai, L. M.; Wang, Z. L. Characteristics of output voltage and current of integrated nanogenerators. *Appl. Phys. Lett.* **2009**, *94*, 022905.

[34] Chen, T.; Barton, S. C.; Binyamin, G.; Gao, Z. Q.; Zhang, Y. C.; Kim, H. H.; Heller, A. A miniature biofuel cell. *J. Am. Chem. Soc.* **2001**, *123*, 8630–8631.

[35] Coman, V.; Ludwig, R.; Harreither, W.; Haltrich, D.; Gorton, L.; Ruzgas, T.; Shleev, S. A direct electron transfer-based glucose/oxygen biofuel cell operating in human serum. *Fuel Cells* **2010**, *10*, 9–16.